Using 1-D Models to Interpret the Reflectance Anisotropy of 3-D Canopy Targets: Issues and Caveats

Jean-Luc Widlowski, Bernard Pinty, Thomas Lavergne, Michel Max Verstraete, *Senior Member, IEEE*, and Nadine Gobron, *Member, IEEE*

***Abstract*—This paper evaluates 1) to what extent one-dimensional (1-D) models can be used to represent the magnitude and directionality of the surface reflectance field of heterogeneous canopy targets at different spatial resolutions, and 2) whether this usage results in significant biases in the estimation of the corresponding state variables. It will be seen that when both the 1-D and three-dimensional (3-D) models account for all features of the measured radiation field, then—in the absence of further information regarding the nature and structure of the target—the use of a 3-D model may amount to an over-interpretation of the available data. The simplified surface structure formulation contained within the 1-D model, on the other hand, may affect the values of the state variables that such models will retrieve. This is because the shape of the reflectance anisotropy of the 3-D target is almost always different from that of a structurally homogeneous (1-D) canopy with the same state variable values but no foliage clumping. By consequence the 1-D canopies that are capable of mimicking the bell (or bowl) shaped reflectance anisotropy of 3-D targets will tend to feature lower leaf area index, higher soil albedo and, in particular, predominantly erectophile (or plagiophile) leaf normal distributions.**

***Index Terms*—Bidirectional reflectance function (BRF) shape, multiangular reflectance data, one-dimensional (1-D) models, pixel-based inversion, three-dimensional (3-D) canopy structure.**

I. Introduction

SURFACE heterogeneity exists at many different spatial scales and affects both the structural and spectral properties of vegetated targets. In addition, canopy characteristics do not remain constant in time, but tend to evolve under the influence of phenological processes, anthropological activities, canopy aging, and natural hazards, to mention but a few. As a consequence, both the magnitude and directionality of the reflectance signature of vegetated surfaces is continually changing, and depends not only on the illumination and viewing directions, but also on the structural (and spectral) composition of the target area and its surroundings at the time of measurement. Furthermore, space borne sensors are constrained to deliver spatially integrated quantities pertaining to the *ensemble* of objects that are located within their instantaneous field of view (IFOV), which—for global missions—tends to be significantly larger than the typical dimensions of structural and spectral surface properties that are present within the observed biophysical systems.

Improvements in Earth Observation, in particular with the advent of multiangular sensors [1]–[4], have stimulated advances in the development of better radiative transfer (RT) models, especially to account for the anisotropy of the reflected radiation fields and to describe the role of the structure and properties of the complex systems that are being observed. Indeed, the dependency of the reflectance of a target on the observation angles (zenith and azimuth) has been explicitly linked to both the intrinsic optical properties of the materials and the geometric structure of the target (e.g., gappiness) [5]–[9].

The characterization of this surface heterogeneity can, however, be considered meaningful only if the surface properties of the observed 3-D target area cause its reflectance field to deviate noticeably from that of structurally dissimilar but otherwise (i.e., in terms of state variables) identical counterparts. If this is not the case, then a large variety of potential surface type candidates, having different structural and spectral properties, will all become equally probable on the basis of the available bidirectional reflectance factor (BRF) measurements alone. The most extreme situation that can thus arise is when a set of multispectral and multidirectional BRF data can be interpreted equally well by RT model simulations using 1) plane parallel canopy representations, with no scales of organization beyond the individual leaf (1-D), and 2) heterogeneous canopy representation, with an entire hierarchy of physical scales from the individual leaf to entire patches of forest (3-D). If both the 1-D and 3-D RT models are capable of explaining the target's BRF pattern—in the sense that differences between either model simulations and the data are smaller than the user-prescribed accuracy requirements, or well within the expected uncertainties of the measurements and/or model limitations—then the retrieval of heterogeneous (3-D) surface information from that set of BRF measurements may denote an over-interpretation of the available data and should (if at all) be conducted with caution. On the other hand, the interpretation of the state variable values of the 1-D model may also constitute a challenging task, since it is well known, both in cloud and vegetation canopy physics, that structural oversimplifications and misrepresentations of the geophysical media of interest may lead to (sets of) state variable values that have little bearing on reality, e.g., [10]–[15].

This paper investigates two issues regarding the interpretation of optical remote sensing data over land using physically based RT models. The first one concerns the ability of structurally

Manuscript received December 2, 2004; revised April 22, 2005.

The authors are with the Joint Research Centre of the European Commission, Institute of the Environment and Sustainability, 21020 Ispra, Italy (e-mail: jean-luc.widlowski@jrc.it).

Digital Object Identifier 10.1109/TGRS.2005.853718

simple RT models (i.e., 1-D) to represent the anisotropy of a reflectance field generated by a more complex 3-D model at multiple spatial resolutions. In other words, when and to what extent are 1-D models—with their ecologically improbable canopy architectures—capable of representing the reflectance anisotropy of complex forest scenes? As soon as the structurally simplest (1-D) model is able to match the reflectance field over complex 3-D plant architectures, then—without *a priori* information on the target—it will no longer be possible to identify the target's true surface structure at the moment of the BRF acquisition. This is because that same set of BRF measurements can always be matched (to within identical accuracy levels) by RT models featuring more involved canopy architecture formulations (i.e., by using more input parameters). Thus in order to select "one" of these surface type solutions for further interpretation efforts, the principle of parsimony may be invoked, which—by stating that plurality should not be posited without necessity—would favor the selection of the structurally simplest (1-D) solution in this context. This choice, however, raises a second issue, namely: If a 1-D model can match the BRF field generated by a 3-D model within a predefined range of accuracy, will the inversion of this 1-D model (at low spatial resolution where they are more appropriate) lead to systematic (and significant) biases in the retrieval of surface properties? Both questions are essential in defining the domain of applicability of 3-D RT models in typical remote sensing applications, as well as the kind of errors that can be expected when interpreting optical remote sensing data using 1-D or 3-D surface type candidates that are structurally dissimilar from the observed target.

Section II describes the simulation of the BRF fields for the 3-D target canopies, the generation of a large ensemble of 1-D candidate reflectance fields, and a metric allowing to determine the equivalence between the BRF simulations of a 1-D candidate surface type and the 3-D target. Section III will quantify how well 1-D models are capable of mimicking multiangular BRF simulations over 3-D canopy targets at multiple spatial resolutions. Section IV will subsequently show, that the 1-D solution that is "most suited" to mimick the reflectance anisotropy of the 3-D targets does, however, in general not correspond to the 1-D candidate with identical state variable values as the target. The properties of the state variable values of the "BRF-equivalent" 1-D surface types will then be documented in Section V, whereas Section VI discusses some of the consequences and implications of these findings.

II. Experimental Setup

In order to simulate very high spatial resolution reflectance fields at multiple field of view locations within a larger heterogeneous surface representation, in an accurate and computationally efficient manner, the 3-D Monte Carlo raytracing model of [16] was expanded using the local estimator (or *photon spreading*) technique described, for example, in [17] to yield the Rayspread model [18]. Simulations of the homogeneous and heterogeneous test cases of the RAMI benchmarking project (http://rami-benchmark.jrc.it) agreed within 0.01% of those of [16]. Specifically, the Rayspread model was applied to the simulation of multiangular and multispectral surface BRF $(\rho_{3\mathrm{D}})$ measurements acquired with an ideal sensor over coniferous forest representations at multiple spatial resolutions.

TABLE I
Structural and Optical Properties of the 94 506 Structurally Homogeneous (1-D) Surface Types in the Lookup Tables

Parameter	Value(s)
Canopy Height [m]	12
Leaf Radius [m]	0.0125
Leaf Area Index	0.0, 0.1 - 7.5 (in steps of 0.1)
Leaf Normal Distr.	uniform*, planophile, plagiophile, extremophile, erectophile
Leaf Reflectance (Red)	0.005, 0.01 - 0.06 (in steps of 0.01)
Leaf Transmittance (Red)	0.005, 0.01 - 0.06 (in steps of 0.01)
Leaf Reflectance (NIR)	0.39 - 0.51 (in steps of 0.02)
Leaf Transmittance (NIR)	0.37 - 0.49 (in steps of 0.02)
Soil Albedo (Red)	0.072, 0.126*, 0.172, 0.238, 0.299, 0.351
Soil Albedo (NIR)	0.084, 0.159*, 0.207, 0.292, 0.356, 0.428
Scattering Law*	Lambertian (for soil) Bi-Lambertian (for leaves)

* Value(s) also used for 3-D surface representations.

The vertically elongated crown shapes and the low needle reflectance and transmission values of this biome were deemed likely to force the anisotropy of the reflectance field to deviate quickly from that of a structurally homogeneous surface. The selection of the architectural properties of individual trees capitalized on the compilation of allometric relationships described by [19], to yield Scots Pine (*Pinus Sylvestris*) stands with a uniform spatial distribution, a lognormal tree height distribution having a mean tree height of 12 ± 1 m, an average crown leaf area index (LAI) of 3.37 ± 0.16, and four different tree density values, namely, 300, 600, 1200, and 1800 stems per hectare. For each one of these 3-D forest scenes the outer scene dimension (S^D) was set to 900 m and the entire canopy was illuminated in a uniform manner. This was to ensure a proper representation of the horizontal fluxes across the lateral boundaries of the sampled canopy volume at all spatial resolutions of interest. Local BRF simulations were performed at various spatial resolutions $(1\,\mathrm{m} \leq S \leq 500\,\mathrm{m})$ and for multiple footprint locations, $\mathbf{R} = (x, y, z^{\mathrm{TOC}})$ contained within the spatial extent of the overall forest scenes. The top-of-canopy BRFs were computed for seven out of the nine nominal view zenith angles of the Multiangle Imaging SpectroRadiometer (MISR) onboard Terra ($\theta_v = 0°$, $\pm 26.1°$, $\pm 45.6°$, $\pm 60.0°$) in both the orthogonal and principal plane, for the red and near-infrared (NIR) spectral bands, and for an illumination zenith angle of $\theta_0 = 30°$. The reference height for the BRF simulations was kept at a constant height $z^{\mathrm{TOC}}(S^D)$, chosen to be slightly larger than the maximum tree height encountered within the overall forest representations.

In parallel, a series of lookup tables (LUTs) was generated, using the semidiscrete 1-D model of [20], that contain the reflectance fields $\rho_{1\mathrm{D}}^m$ of a large number $(m = 1, \ldots, M = 94\,506)$ of structurally homogeneous surface types under the same conditions of illumination, $\mathbf{\Omega}_0 = (\theta_0, \phi_0)$ and observation, $\mathbf{\Omega}_v = (\theta_v, \phi_v)$ as for the 3-D cases. The structural and spectral properties of the various 1-D canopy types in the LUT are summarized in Table I. Their reflectance fields are assumed to be representative of the entire domain of solutions that structurally homogeneous vegetation canopies can exhibit (when simulated by the semidiscrete RT model). Finally, in an effort to assess the level of uncertainty arising from different radiation transfer implementations, both the Rayspread (3-D) and the semidiscrete (1-D) RT models

simulated the reflectance fields of structurally homogeneous (1-D) vegetation canopies with low (0.25) and high (7.00) LAI values. The resulting model-induced uncertainty levels in the orthogonal (principal) plane were 0.76 (0.69)% and 0.56 (7.39)% of the BRFs in the red, as well as 0.25 (0.52)% and 0.09 (0.44)% of the BRFs in the NIR, for the low and high LAI values respectively.

At any given spatial resolution of interest and for each one of the various footprint locations within the 900×900 m^2 Scots Pine forest, the local 3-D BRF field is then compared against all 94 506 candidates in the 1-D LUT and the closest matching 1-D solution is identified. More specifically, the radiative separation between BRF measurements gathered with a spatial resolution S from position $\mathbf{R}$ above a 3-D forest target illuminated along direction $\mathbf{\Omega}_0$, and their radiatively most alike counterpart from amongst the ensemble of 1-D surface types in the LUT is computed as follows. First, the maximum difference between $\rho_{3D}^{S,\mathbf{R}}$ and ρ_{1D}^{m} over the set of available view directions $\mathbf{\Omega}_v^k (k = 1, \ldots, K)$ and spectral bands $\lambda_\ell (\ell = 1, \ldots, L)$ has to be determined for each one of the M different 1-D surface types in the LUTs. Then, in a second step, the minimum difference value out of this set of M potential candidates is selected and termed the *radiative separability limit*, $\epsilon(S, \mathbf{R}; \mathbf{\Omega}_0, K, L, M)$. Formally,

$$\epsilon(S, \mathbf{R}; \mathbf{\Omega}_0, K, L, M) = \mathrm{Min}\left[\mathrm{Max}\left[\frac{\left|\rho_{3D}^{S,\mathbf{R}}\left(\mathbf{\Omega}_v^k, \lambda_\ell\right) - \rho_{1D}^{m}\left(\mathbf{\Omega}_v^k, \lambda_\ell\right)\right|}{0.01\rho_{3D}^{S,\mathbf{R}}\left(\mathbf{\Omega}_v^k, \lambda_\ell\right)}\right]_{K,L}\right]_{M}. \quad (1)$$

The value of $\epsilon(S, \mathbf{R}; \mathbf{\Omega}_0, K, L, M)$ identifies the tolerance-of-fit threshold (as a percentage of the 3-D BRF values) beyond which at least one of the M different 1-D surface types in the LUTs is capable of explaining the entire set of K multiangular and L multispectral BRF observations gathered with a spatial resolution S at location $\mathbf{R}$ above a 3-D forest scene that is illuminated along direction $\mathbf{\Omega}_0$. In other words, ϵ describes the smallest possible envelope (expressed as a percentage of the 3-D BRFs) that can be drawn around the BRF data of both the 3-D target and one of the M different 1-D candidates in the LUT. Although the value of this radiative separability limit $\epsilon(S, \mathbf{R}; \mathbf{\Omega}_0, K, L, M)$ is always dependent on the particular viewing and illumination conditions, as well as on the amount of available spectral bands and 1-D solutions in the LUT, these dependencies are systematically omitted here since all of K, L, M, and also $\mathbf{\Omega}_0$ were kept constant within this study. Furthermore, to obtain more tractable results, $\epsilon(S, \mathbf{R})$ is averaged over many different footprint locations above the 3-D forest scene to yield the mean radiative separability limit at that spatial resolution: $\bar{\epsilon}(S)$, located somewhere between $\epsilon^{\min}(S, \mathbf{R}')$ and $\epsilon^{\max}(S, \mathbf{R}'')$, the minimum and maximum radiative separability values (occurring at some IFOV locations $\mathbf{R}'$ and $\mathbf{R}''$, respectively) at that spatial resolution.

III. Radiative Separability Limit Across Multiple Spatial Resolutions

Fig. 1 shows the minimum $\epsilon^{\min}$ (dotted lines), maximum $\epsilon^{\max}$ (dashed lines) and mean $\bar{\epsilon}$ (solid lines) radiative separability limits obtained from multiangular simulations in the orthogonal plane above structurally heterogeneous Scots Pine forests at spatial resolutions ranging from $1 \leq S \leq 500$ m in the red spectral band. Results are shown for four different tree density values, namely, 300 (red), 600 (black), 1200 (green), and 1800 (blue) stem/ha. It can be seen that both the maximum and mean radiative separability limits are much larger at fine than at coarse spatial resolutions. On the other hand, $\epsilon^{\min}$ remains very small—albeit never exactly zero—across all simulated spatial resolutions and this irrespective of the structure of the 3-D forest type. In particular, one should note that the values of $\epsilon^{\min}$ are always somewhat higher than the model-induced uncertainty of the Rayspread and semidiscrete models mentioned previously.

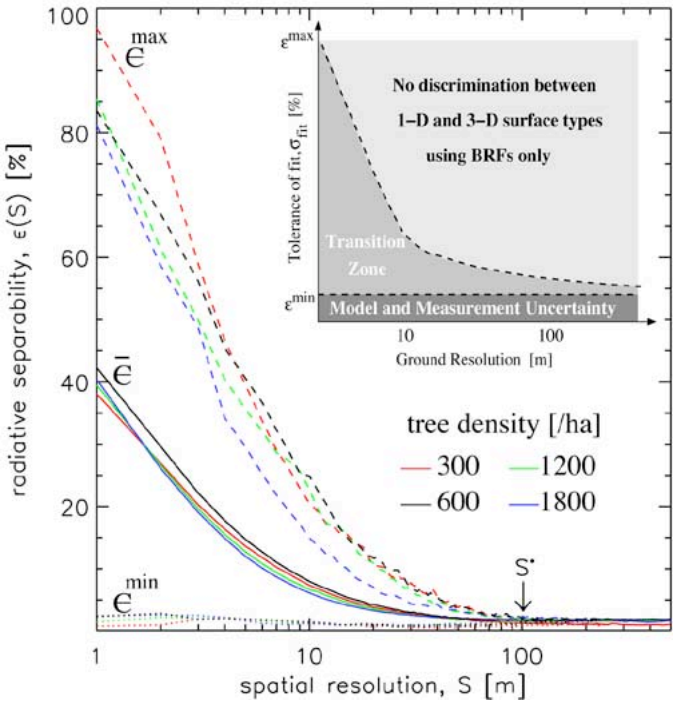

Fig. 1. Maximum $\epsilon^{\max}$ (dashed), minimum $\epsilon^{\min}$ (dotted), and mean $\bar{\epsilon}$ (solid line) radiative separability limits obtained by comparing sets of seven BRF values from 3-D Scots pine representations with their radiatively most alike 1-D counterparts, using different footprint locations and spatial resolutions: 1 m $\leq S \leq$ 500 m in the red spectral band. Results are displayed for BRF simulations in the orthogonal plane, a solar zenith angle $\theta_0 = 30°$, and four different stem densities of the 3-D forest—i.e., 300 (red), 600 (black), 1200 (green), and 1800 (blue) stem/ha—having statistics that are conserved at the hectare level ($S^* = 100$ m).

The decrease of $\epsilon^{\max}$ (and thus also $\bar{\epsilon}$) with increasing field of view of the observing sensor is easily understood, since the reflectance anisotropy over a vast expanse of structurally similar surface targets is not expected to change much between different footprint locations if the spatial resolution of the observing sensor is coarse enough (with respect to the size of the observed structures). Furthermore, since the tree density of the various Scots Pine forest scenes was maintained at the hectare level ($S^* = 100$ m), their structural characteristics are expected to vary very little between different footprint locations when the spatial resolution exceeds 100 m. Assessments of the variability of the LAI values of individual IFOV patches showed that for spatial resolutions of $S > S^*$ the various $\mathrm{LAI}_{3D}(S, \mathbf{R})$ converged rapidly to $\mathrm{LAI}_{3D}(S^D)$, the leaf area index of the 3-D forest at its largest simulated extent ($S_D = 900$ m). In ad-

dition, simulations (not displayed) showed that less than 1% (2.5%) of the reflected photons in the red (NIR) travel distances larger than 100 m between their point of entry and exit at the top of the canopy (z^{TOC}). The 'flattening' of the various $\bar{\epsilon}(S)$ curves in Fig. 1 is thus a direct consequence of the preservation of the "target statistics" at spatial resolutions $S^* \leq S \leq S_D$, such that for large expanses of structurally identical forest types $\lim_{S \to S_D} \epsilon(S, \mathbf{R}) = \bar{\epsilon}(S_D)$.

At very small IFOVs, on the other hand, when the typical sizes of the observed structures (or gaps between them) become comparable to (or even larger than) the nominal footprint width of the sensor, the BRF values gathered at any individual pixel location depend both on what is contained within the footprint area and what is adjacent to it. This phenomenon—which is referred to as the "adjacency effect" in the remote sensing community—arises from alterations in the magnitude and directionality of the horizontal photon flux that enters the volume of interest from (gaps in) neighboring canopy regions. As the spatial resolution of interest becomes higher, both the LAI and structure content of adjacent canopy volumes tend to deviate from their domain-averaged (S_D) statistics. At the same time the relative impact of the lateral photon influx increases with respect to the surface leaving radiation field at the location of the IFOV. Very complex 3-D situations can thus arise, for example, if a small footprint area covers only one or two of a group of tall trees with the (partially shaded) soil being observed below. Such configurations give rise to very distinct reflectance anisotropy shapes that can only be matched by 1-D surface types if the BRF fitting tolerance is sufficiently loose ($\epsilon^{\max} \approx 100\%$ at 1-m spatial resolution in the case of the 300 tree/hectare forest in Fig. 1). On the other hand, if the small footprint area were to fall exactly between the tree crowns of a forest stand, such that it would only cover bare soil, then the radiative separability between 1-D and 3-D surfaces would be substantially reduced, albeit not completely eliminated due to possible shadows and diffuse illumination components from adjacent areas ($\epsilon^{\min} \approx 1\%$ at 1-m spatial resolution in the case of the 300 stem/ha forest in Fig. 1).

The inlaid graph in Fig. 1 shows a conceptual representation of the resolution dependent bias that exists between the BRF fields of *one* 3-D forest representation (standing for the truth) and an extensive set of 1-D candidate surfaces. All combinations of accuracy requirements (σ_{fit}) and sensor spatial resolutions (S) that fall within the (light gray) BRF equivalence region, i.e., $\sigma_{\mathrm{fit}} > \epsilon^{\max}(S)$, imply that a structurally homogeneous vegetation canopy can *always* be found that fits the set of available multiangular (and multispectral) BRF measurements. On the other hand, if the user-specified tolerance of fit criteria fall within the (medium gray) transition zone, i.e., $\epsilon^{\min}(S) \leq \sigma_{\mathrm{fit}} \leq \epsilon^{\max}(S)$, then the validity of the 1-D assumption is subject to the exact placement of the sensor's footprint area with respect to the constituents of the 3-D forest scene. Finally, in situations where σ_{fit} is less than $\epsilon^{\min}(S)$ but larger than the (dark gray) modeling and measurement uncertainty region, then the usage of 3-D RT models is required to match the set of available BRF measurements at the user-specified accuracy requirements. Our BRF simulations in the red (and NIR) spectral band showed, however, that for observation conditions outside the hot spot region both the $\epsilon^{\min}(S)$ and the upper modeling and measurement uncertainty limit are very similar in magnitude. Hence the conceptual graph in Fig. 1 does not feature this exclusion zone of 1-D models.

Additional studies (not shown) with respect to soil brightness conditions, crown LAI, and illumination angle in both the red and NIR showed little effect, whether on the range $(\epsilon^{\max} - \epsilon^{\min})$ and mean values of ϵ, or on their behavior as a function of spatial resolution. In general, the values of $\epsilon^{\max}$ were larger for observations in the principal rather than in the orthogonal plane. This is due to a partial sampling of the hot spot effect [21]–[23], whose measurable angular width is due to the typical sizes of the individual scatterers (leaves) in the 1-D canopies, whereas, in 3-D forest representations, it is controlled primarily by the tree level structures and the gaps between them, e.g., [24]–[26]. Although not shown, simulations in the NIR featured similar patterns as those observed in the red albeit at somewhat lower magnitudes of $\epsilon(S)$. Conversely, when applying (1) to multiangular data in both the red and NIR together, the magnitude of $\epsilon(S)$ increases (in particular at the higher spatial resolutions) although the trends for $\epsilon^{\max}$ and $\epsilon^{\min}$ remain the same.

IV. Angular Signature of 3-D Canopies and Their 1-D Homologues

For the current fleet of medium spatial resolution sensors (e.g., ATSR, MERIS, MISR, MODIS, VEGETATION) it is thus primarily the domain-averaged structural and spectral characteristics of a 3-D target that determine the magnitude and angular shape of its surface leaving reflectance field—provided that the target under observation is embedded within a larger area with similar properties. Under these conditions, [27] noticed that highly heterogeneous targets possess different BRF shapes than their independent pixel approximation *(IPA) homologues*. The latter are linear combinations of RT simulations using 1-D representations of bare soils and foliage canopies with identical spectral and structural leaf properties (including the leaf area density) as their corresponding 3-D target. These results were obtained by decomposing the IPA reflectance field into an amplitude term and a shape function, for which the modified Minnaert function parameter k describes the degree of bell $(k > 1)$ or bowl $(k < 1)$ shape of the anisotropy [28]. For multiangular observations outside the principal plane it was found that, the bell-shaped reflectance anisotropy arising (in particular at medium to small solar zenith angles) over 3-D targets—preferrably those with intermediate vegetation content and high background brightness—had a tendency to be more pronounced than that of their corresponding IPA homologues.

Rather than using IPA homologues, this contribution will compare the Minnaert function parameter of 3-D targets against that of their 1-D homologues instead. The *1-D homologue* of a 3-D target is a structurally homogeneous vegetation canopy that features identical leaf and soil properties (both spectral and structural) as its 3-D original—with the exception of the spatial distribution (and thus by consequence also the leaf area density) of the canopy foliage, which is never clumped. In Fig. 2 the ratio of the Minnaert function parameter of a 3-D target $(k_{3\mathrm{D}})$ and its 1-D homologue $(k^*_{1\mathrm{D}})$ is plotted for 350 structurally diverse forest scenarios in both the red and NIR spectral bands. The canopy architectures were generated using the allometric relationships compiled by [19], and feature predominantly random distribution of trees of various sizes and shapes. These

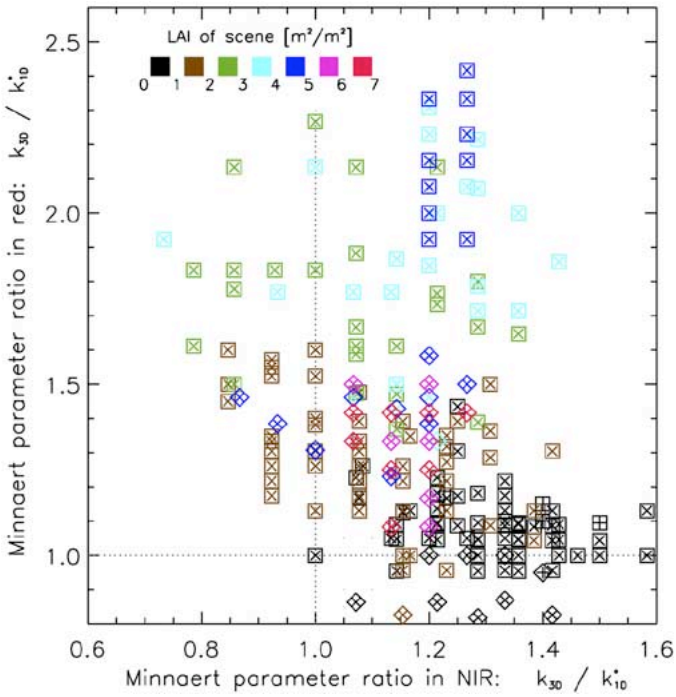

Fig. 2. Ratio of the modified Minnaert function parameters obtained from the reflectance anisotropy shape of 350 heterogeneous forest scenes (k_{3D}) and their corresponding 1-D homologue (k^*_{1D}) in the red and NIR spectral band if $\theta_0 = 30°$. k_{3D} varied between 0.60 (0.55) and 1.7 (1.1) in the red (NIR) spectral band. In the red (NIR) spectral band, bell-shaped reflectance patterns—having $k_{3D} > 1$—are indicated by a $\square$ $(+)$ symbol, whereas Lambertian or bowl-shaped reflectance patterns—having $k_{3D} \leq 1$—are displayed with a $\Diamond$ $(\times)$ symbol, respectively.

forest scenes contain also, however, a non-negligible number of scenarios featuring non-random tree distributions—in order to simulate forest clearings and small groves—and scenes with various amounts of "dead trees," i.e., trees having no foliage (see Table II for further details). The surface-leaving BRF field of the 3-D forest representations was simulated using a medium soil brightness, an illumination zenith angle of 30°, and a sensor spatial resolution of 250 m. Using the approach of [29], the Minnaert function parameter, k was retrieved from seven BRF observations in the orthogonal plane. The most likely values of the retrieved k_{3D} parameters varied between 0.60 (0.55) and 1.7 (1.1) in the red (NIR) spectral band. In Fig. 2 most of the heterogeneous forest scenes feature elevated k values when compared to their 1-D homologues and this irrespective of the spectral band. In particular in the red spectral band, where soil backscattering dominates over leaf scattering, the gaps between the trees of the 3-D canopy contribute toward increased BRF values at small view zenith angles whereas the amount of radiation that exits the scene at larger zenith angles is effectively reduced by the presence of densely packed foliage within the tree crowns. As a consequence, 3-D vegetation canopies tend to feature enhanced degrees of bell-shaped reflectance anisotropies when compared to their 1-D homologues, in particular for intermediate values of LAI. In the NIR, where leaf scattering dominates over background scattering, the situation is somewhat more complicated since the multiple scattering contribution is substantially enhanced with respect to its counterpart in the red (up to 35% of the total) and may assume either a bowl, or, a bell shape depending on the soil

TABLE II
STRUCTURAL PROPERTIES OF 350 HETEROGENEOUS FOREST CANOPIES

Parameter	Range
Crown Volume [m^3/ha]	0 - 59724
Gap Fraction [%]	11.6 - 98.2
Mean Canopy Height [m]	4.29 - 24.49
Mean Tree Spacing [m]	0.75 - 25.29
Leaf Area Index [m^2/m^2]	0.00 - 6.76
Tree Density (live) [stems/ha]	8 - 8644
Tree Density (dead) [stems/ha]	34 - 1634
Trunk Volume [m^3/ha]	1.02 - 632.42

brightness, vegetation density and illumination conditions that prevail, e.g., [15].

A direct consequence of the difference between the shapes of the anisotropies ($k_{3D} \neq k^*_{1D}$) is that the 1-D homologue of a 3-D target will almost certainly not be identified as the best matching 1-D candidate—as defined by (1)—in a LUT-based inversion scheme trying to match multiangular BRF measurements without any *a priori* knowledge regarding the structure of the underlying target. For example, the mean separability limit of the various 3-D Scots Pine scenes without "dead trees" in Fig. 2 was found to be $1.70 \pm 0.80\%$ in the red, and $0.91 \pm 0.33\%$ in the NIR, with no value of ϵ exceeding 6% in the red and 4% in the NIR. The radiative separability limit between these 3-D forest scenes and their corresponding 1-D homologue (ϵ^*), on the other hand, was always found to be at least twice as large, i.e., ϵ/ϵ^* was 0.5 or less in both the red or NIR spectral domain. With such evidence at hand, it is likely that the structural differences that exist between the various 3-D Scots pine representations described in Table II and their 1-D homologues are sufficient to prevent them from exhibiting identical reflectance fields, and therefore also transmission and absorption fluxes. On the other hand, it is always possible to identify—structurally and spectrally dissimilar—1-D candidates that are capable of mimicking the outgoing reflectance field of the 3-D target. The next section is going to investigate the properties of such *BRF-equivalent* 1-D solutions by comparing them with their 1-D homologues.

V. PROPERTIES OF BRF-EQUIVALENT 1-D CANOPIES AT COARSE RESOLUTIONS

Being able to mimick the magnitude and directionality of the surface leaving radiation field with a 1-D RT model does, however, not imply that the other components of the radiation budget, i.e., absorption and transmission, are matched equally well, nor that the retrieved values of the state variables in the RT model which permitted the fitting actually correspond to the real values of the 3-D target. Fig. 3 highlights this point by showing, that for the same 350 Scots Pine forests as in Fig. 2 ($\theta_0 = 30°$), the BRF-equivalent 1-D candidate [in the sense of (1)] is quite capable of matching the magnitude of the spectral albedo $(\bullet)$ of the 3-D forest target. The canopy absorption $(+)$ of the selected 1-D solution from the LUT is, however, far less well resolved, both in the red (top panel) and NIR (bottom panel) spectral bands. In the red spectral band the scatter in the absorption data increases as the 3-D canopies exhibit lower absorption values, and this predominantly through an overestimation of the absorption by the structurally homogeneous canopies. Exceptions to this occur for very dense vegetation canopies, where the LAI $_{3D}$

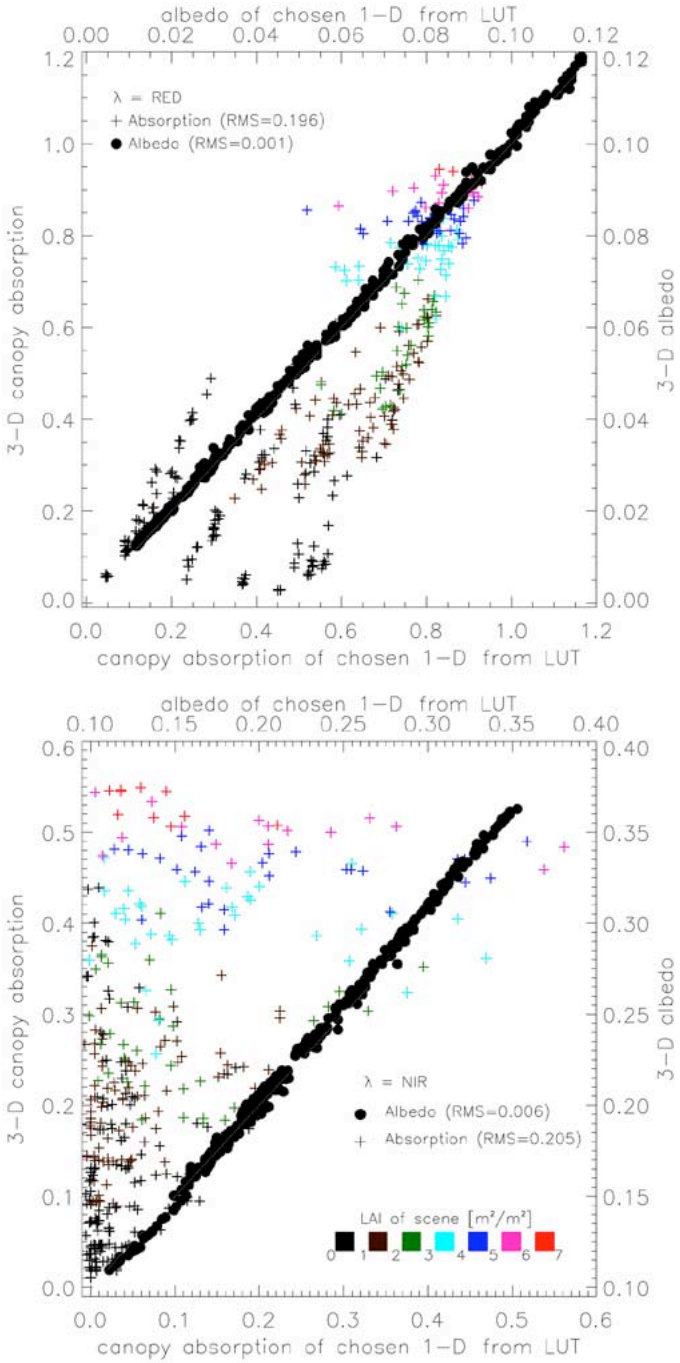

Fig. 3. Albedo (●) and canopy absorption (+) of the same 350 Scots Pine forest scenes as in Fig. 2 ($\theta_0 = 30°$), plotted against the corresponding value of their radiatively most alike 1-D vegetation canopy identified—using (1)—from observations along the orthogonal plane in (top panel) the red and (bottom panel) NIR spectral bands. In the case of absorption data, the color scheme identifies the LAI of the 3-D scene.

is such that the corresponding 1-D homologue exceeds the theoretical limit for semi-infinite vegetation canopies (i.e., LAI ~ 4) [30], and for 3-D canopies with relatively low LAI values featuring a substantial number of "dead trees." Here the large fraction of woody elements enhances the (3-D) canopy interception and thus also its absorption, whereas—as a consequence of energy conservation—the transmission values of these 3-D canopies will be inferior to those of the selected 1-D canopies. In the NIR, on the other hand, the chosen 1-D solutions systematically underestimate the canopy absorption of their 3-D targets, a situation that is exacerbated as the LAI (and woody fraction) of the heterogeneous canopy increases. As such the interpretation of optical remote sensing data with structurally incorrect canopy candidates may lead to errors in the estimation of the canopy absorption that, in the red spectral band, feature a root mean square (RMS) error of 0.229, 0.215, 0.187, 0.089, 0.094, and 0.098 for successive LAI classes (of width 1) ranging up to 1, 2, 3, 4, 5, and 6 m ^{2}/m^2, respectively.

Such findings are, however, not surprising since the selection of the BRF-equivalent 1-D surface type was entirely driven by its capability of mimicking the outgoing reflectance field of the 3-D target, and not with respect to a correct redistribution of the incoming solar radiation into a transmitted and absorbed energy component [15]. Obviously, the need of the 1-D canopies to compensate for the somewhat brighter reflectance of the trunks and branches in the 3-D forest scenes, the predefined range and intervals of the solutions in the LUT, and the selected criteria for identifying the "best matching" 1-D candidate all may contribute to the observed discrepancies in Fig. 3. Nevertheless, the fact remains that even an (almost) perfect match of the reflectance anisotropy of a 3-D target may still lead to erroneous estimates of parameters—like the fraction of absorbed radiation by the canopy—simply because of the structural differences that exist between the modeled and observed surface types. In effect, the various state variables in a 1-D RT model are forced to adopt values that may very well deviate from reality because they have to compensate for the imposed vegetation structure whilst the inversion routine attempts to minimize the differences with the BRF data of the 3-D target. In Fig. 2 it was shown that the 3-D targets, described in Table II, tended to exhibit reflectance anisotropies with enhanced bell shapes in the red and less pronounced bowl shapes in the NIR than their 1-D homologues ($k_{3D} \geq k^*_{1D}$). Hence, the BRF-equivalent 1-D solution to multiangular observations of a 3-D target will thus have to feature enhanced (reduced) BRF values at low view zenith angles θ_v, and equal or reduced (enhanced) BRF values at large θ_v when compared to the 1-D homologue of the 3-D target in the red (NIR) spectral band. Since soil backscattering tends to dominate over leaf scattering in the red, enhanced reflectance values at small θ_v can be achieved by brighter soils, increases in the bare soil fractions at these zenith angles, or combinations of both of these. Furthermore, to achieve a more pronounced bell shape of the reflectance field, the upward reflected radiation from the soil has to be prevented from exiting at larger view zenith angles. This can be achieved by reducing the single-scattering albedos of the leaves, and by enhancing the extinction coefficient along large θ_v directions. [31] showed that canopies with predominantly erectophile leaf orientations present a larger (lower) interception cross-section to photons that travel at large (small) zenith angles. Hence, it is most likely that 1-D canopies will adopt erectophile leaf normal distributions when mimicking bell-shaped reflectance anisotropies. This is indeed confirmed by the findings presented in the top panel of Fig. 4.

In the NIR where leaf scattering dominates over the soil scattering properties, enhanced BRF values at larger view zenith angles can be obtained through foliage orientations that effectively redirect upward reflected radiation into surface-leaving

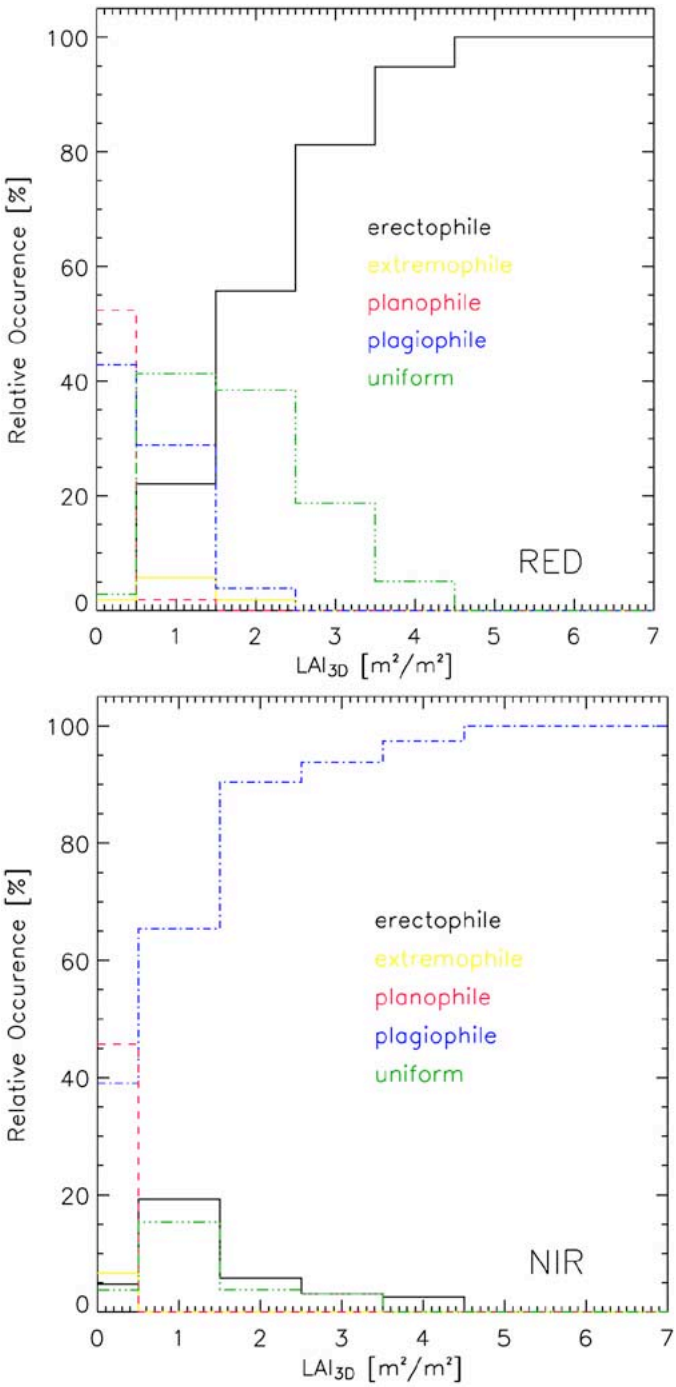

Fig. 4. Percentage of the various leaf normal distributions (erectophile, extremophile, plagiophile, uniform, and planophile) adopted by the best matching 1-D solutions capable of accurately mimicking the surface-leaving reflectance field of 350 structurally diverse 3-D forest canopies in (top panel) the red and (bottom panel) NIR spectral bands. The 3-D scenes featured a uniform leaf normal distribution.

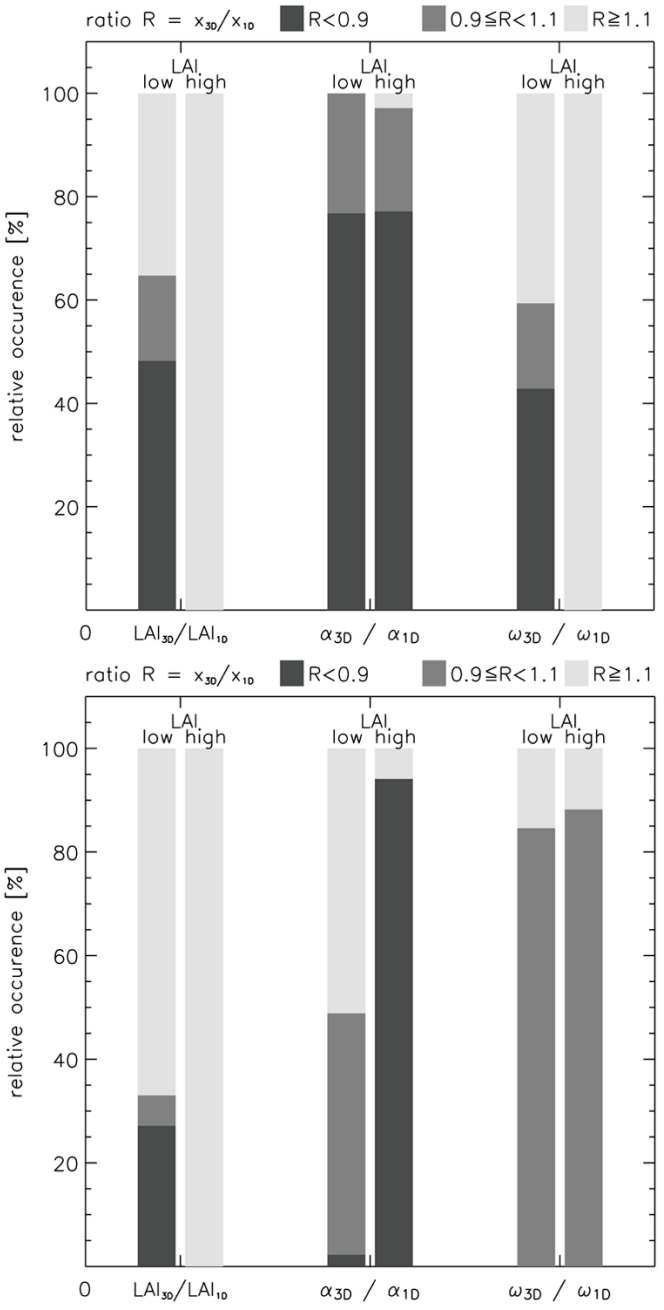

Fig. 5. Ratio R of the "true" (3-D) to "BRF-equivalent" (1-D) state variable values for LAI, soil albedo (α), and single-scattering albedo (ω) grouped into categories of low $(\mathrm{LAI_{3D}} < 2.3)$ and high $(\mathrm{LAI_{3D}} > 4.6)$ vegetation content, in both (top panel) the red and (bottom panel) NIR spectral bands. A light (dark) gray color indicates that the 1-D state variable values were significantly smaller (larger) than those of the 3-D target. A medium gray color indicates that the values of the 1-D solution were within 10% of those of the 3-D target.

directions corresponding to larger view zenith values. Such a mechanism would, however, require sufficient amounts of light to reach the background and then to be scattered back upward into the vegetation from the underlying surface. Again, [31] describes two types of foliage orientations that feature enhanced (reduced) extinction cross sections at small (large) zenith angles, these being the planophile and plagiophile leaf normal distributions (LND). The bottom panel in Fig. 4 shows that it was, however, the plagiophile LND that was preferentially adopted by the best matching 1-D solution. This could be related to the fact that the interception cross-section, $G(\mathbf{\Omega})$ of the planophile LND is rather large at small view zenith angles, thus effectively preventing the radiation from entering the canopy, as well as enhancing the upward reflected radiation fraction at small θ_v—both of which are contrary to the envisaged bowl-shaped reflectance anisotropy.

Fig. 5 provides an indication on how the remaining state variable values of the selected 1-D solution, i.e., LAI, soil albedo

(α) and single-scattering albedo (ω), relate to their counterparts in the 3-D target canopy. Results are displayed in terms of the ratio, R of the "true" (3-D) and the "BRF-equivalent" (1-D) state variable for scenarios featuring either low $(\mathrm{LAI}_{3\mathrm{D}} < 2.3)$ or high $(\mathrm{LAI}_{3\mathrm{D}} > 4.6)$ vegetation content. A light (dark) gray color indicates a significant underestimation (overestimation) of the 1-D state variable values, whereas a medium gray color indicates that the values of the 1-D solution were relatively close to those of the 3-D target. In the red spectral band (top panel) only $\sim$20% of the 1-D state variable values in the low $\mathrm{LAI}_{3\mathrm{D}}$ cases are similar to those of the 3-D target $(0.9 \leq R < 1.1)$. At large LAI values—where the 1-D canopy absorption is relatively close to the 3-D one (compare with Fig. 3)—the agreement is, however, much lower: The LAI of the selected 1-D solution $(LAI_{1\mathrm{D}})$ tends to be smaller than that of the 3-D scenes $(\mathrm{LAI}_{3\mathrm{D}})$ most likely to compensate for the lack of canopy gaps within the structurally homogeneous canopy representations. At the same time the soil albedo $(\alpha_{1\mathrm{D}})$ is brighter thus implying that more light is reflected back up through the canopy as stated previously. Finally the single-scattering albedo $(\omega_{1\mathrm{D}})$ is also lower than its 3-D counterpart to enhance the absorption of the 1-D canopy in particular along directions with larger zenith angles. In the NIR (bottom panel), the single-scattering albedo appears more or less in agreement with the actual values of the 3-D target. However, as described above, it will be primarily the leaf area index, the foliage orientation and soil albedo that control the bell-shaped BRF matching in this spectral regime where multiple scattering interactions dominate. Thus by analogy with the findings of [32]—who fitted noisy multiangular BRF simulations with a 1-D model—the best matching 1-D solution in the NIR underestimates LAI and overestimates soil albedo values for 3-D targets with high vegetation content.

VI. Discussion

It has been shown that 1-D RT models are capable of matching multiangular BRF observations over highly heterogeneous targets to within the accuracy specifications of most current sensors at medium to coarse spatial resolutions. Being able to mimick a set of (multiangular and/or multispectral) reflectance measurements within 3% to 5% may, however, still lead to substantial errors in the estimation of canopy transmission and absorption estimates at these spatial resolutions. Furthermore, the state variable values that are retrieved by pixel-based inversion of 1-D models (or, in general, RT models that do not incorporate the correct canopy structure) will almost always differ from the actual ones of the observed 3-D target. This issue will persist even if *a priori* knowledge is being used: 1) to reduce the amount of potential 3-D surface type candidates that will have to be precomputed for later perusal in LUT-based inversion schemes and 2) to make their state variable values similar to actual field observations of the biome types of interest. Actual forest targets exist in a variety of structural and spectral "states" and as such it is unlikely that the "true" solution will be contained within the candidate solutions in the LUT. But even if one assumes that the LUT is sufficiently large to include the "true" solution, its retrieval will still not be guaranteed, since the sensor and model imposed uncertainties will always allow for multiple model parameter combinations (to be found within the LUT) that all fit the available data.

Furthermore, the accuracy of pixel-based inversion schemes is strongly dependent on the spatial resolution of the observing multiangular sensor since the impact that the structural attributes of an individual tree may have with respect to the surface leaving radiation field is larger at high spatial resolutions than at medium to coarse spatial resolutions. As a consequence, the BRF matching capability of RT model simulations becomes subject to the lateral boundary conditions, and thus also to the given location of the field of view of the observing sensor, as was shown by the drastic increase in the radiative separability limits in Fig. 1 at high spatial resolutions. Conversely, this also implies that validation attempts of state variables—retrieved through the usage of 3-D LUTs containing statistical representations of typical canopy architectures—may run into inconsistencies when compared to findings gathered at much higher spatial resolutions in the field, precisely due to the deterministic nature of the boundary conditions in the latter case.

One of the main paradigms in interpretation efforts of mono-directional optical remote sensing data is to utilize multispectral observations to further constrain any inversion attempts. In the context of multiangular reflectance observations, however, it was shown that 1-D canopies can achieve BRF-equivalence within a few percent (at any one wavelength) provided they adopt different values for their state variables than the 3-D target. The "freezing" of structural attributes—like the LAI and the LND—across multiple wavelengths will thus primarily lead to poorer fitting accuracies (i.e., higher ϵ values) and not necessarily to improved estimates of the retrieved state variables. For example, the RMS error between the actual and retrieved LAI (albedo) values for the 350 forest scenes presented earlier amounted to 1.090 (0.001), 1.978 (0.006) and 1.248 (0.002) if the best matching 1-D candidate was determined from multiangular BRF observations in the red, NIR and both spectral bands together, respectively. Furthermore, by not choosing an erectophile LND in the red spectral band and a plagiophile LND in the NIR to match the occurrence of bell and bowl shaped reflectance patterns at these two wavelengths individually, a multispectral multiangular approach with fixed structural properties will lead to the forced selection of 1-D canopies with somewhat intermediate LNDs, maybe even uniform, which—although being the truth—will only be identified because of a compromise in matching different kinds of reflectance pattern with a structurally simplified or erroneous RT model. This is neither a limitation of the data nor the model, but rather a consequence of the choice of inversion approach and the structural differences between the modeled and observed surface types.

It is important to realize that state variables, obtained by inverting a RT model against BRF measurements over a 3-D target, have to be corrected for the lack, or, incorrectness of structural heterogeneity in between the 3-D target and the retrieved surface type solution. Recent developments in radiation transfer in both vegetation canopies and cloud physics have already shown that it may be possible to interpret remote sensing

observations using plane-parallel RT models provided that the retrieved sets of state variables are subsequently interpreted following some protocol, e.g., [15], [33]–[36]. Such efforts are needed, not only in validation attempts but also to ensure the correct usage of satellite-derived quantitative information in subsequent applications. We have shown that the structural formulation of vegetation canopies within a 1-D RT model affects the values of state variables—like LAI and soil albedo—that can be retrieved by inverting that model against multiangular observations over 3-D forest targets. Any subsequent ingestion of such 1-D state variables into process models, that assume simpler (two stream) or more complex (3-D) canopy structures and radiation schemes, will surely result in a misrepresentation of actual (structural and radiative) conditions at the surface and thereby will cast substantial doubts on simulation results obtained in that way [37]. Thus, if the value of a given state variable depends on the dimensionality of the RT model that was used in its retrieval, then surely this state variable should only be processed further by (process) models and algorithms that imply/feature the same dimensionality in their formalism, or else, correct for the structural assumptions in the RT models used to derive the state variables in the first place [38].

VII. Conclusion

Evidence was provided that structurally homogeneous (1-D) radiation transfer models are capable of mimicking multiangular BRF measurements, in both the red and NIR spectral bands within 3% to 5% at medium to coarse spatial resolution. The fitting accuracy of the 1-D model deteriorates, however, at very high spatial resolutions to reach about 40% on average (in the case of coniferous forests), primarily due to adjacency effects and variable boundary conditions. BRF-equivalency—in terms of the magnitude and angular variation of the surface leaving reflectance field—between a 3-D target and some structurally and spectrally dissimilar candidate solution, on the other hand, does not necessarily guarantee the correct retrieval of other radiative quantities pertaining to the target (e.g., canopy absorption and transmittance), nor does it generally yield state variable values that correspond to those of the 3-D target. For example, in order to mimick the bell (bowl) shaped BRF field of a 3-D target, 1-D canopies will tend to feature brighter soil albedos, lower LAI values, and—most notably—foliage orientations that intercept the surface leaving radiation preferably at large (small) view zenith angles. Structural canopy attributes that are retrieved with 1-D models in either the red or near-infrared spectral bands will thus in all likelihood be different (from each other and from the 3-D target) if the illumination conditions favor the occurence of significantly bowl/bell-shaped BRF fields. Finally, the usage of multispectral information, in inversion techniques that rely only on the matching of multiangular reflectance observations, will not necessarily lead to improved accuracies of the retrieved state variables, but surely loosens the quality of fit between the multispectral BRF fields of the best matching 1-D candidate and the sensor observations. For a proper interpretation of optical remote sensing data, efforts will thus have to be focused on using additional or *a priori* knowledge regarding the degree of heterogeneity of the underlying 3-D target in order to allow for the development of correction schemes that convert "BRF-equivalent" state variable values into those of the 3-D targets.

References

[1] P. Y. Deschamps, F.-M. Bréon, M. Leroy, A. Podaire, A. Bricaud, J.-C. Buriez, and G. Sèze, "The POLDER mission: Instruments characteristics and scientifc objectives," *IEEE Trans. Geosci. Remote Sens.*, vol. 32, no. , pp. 598–615, May 1994.

[2] N. C. M. Stricker, A. Hahne, D. L. Smith, J. Delderfield, M. B. Oliver, and T. Edwards, "ATSR-2: The evolution in its design from ERS-1 to ERS-2," *ESA Bull.*, vol. 83, pp. 32–37, 1995.

[3] D. J. Diner, J. C. Beckert, T. H. Reilly, C. J. Bruegge, J. E. Conel, R. A. Kahn, J. V. Martonchik, T. P. Ackerman, R. Davies, S. A. W. Gerstl, H. R. Gordon, J.-P. Muller, R. B. Myneni, P. J. Sellers, B. Pinty, and M. M. Verstraete, "Multi-angle Imaging Spectroradiometer MISR instrument description and overview," *IEEE Trans. Geosci. Remote Sens.*, vol. 36, no. 4, pp. 1072–1087, Jul. 1998.

[4] M. J. Barnsley, J. J. Settle, M. Cutter, D. Lobb, and F. Teston, "The PROBA/CHRIS mission: A low-cost Smallsat for hyperspectral, multiangle, observations of the earth surface and atmosphere," *IEEE Trans. Geosci. Remote Sens.*, vol. 42, no. 7, pp. 1512–1520, Jul. 2004.

[5] P. R. J. North, "Three-dimensional forest light interaction model using a Monte Carlo method," *IEEE Trans. Geosci. Remote Sens.*, vol. 34, no. 4, pp. 946–956, Jul. 1996.

[6] J.-L. Widlowski, B. Pinty, N. Gobron, M. M. Verstraete, and A. B. Davis, "Characterization of surface heterogeneity detected at the MISR/TERRA subpixel scale," *Geophys. Res. Lett.*, vol. 28, pp. 4639–4642, 2001.

[7] J. L. Lovell and R. D. Graetz, "Analysis of POLDER-ADEOS data for the Australian continent: The relationship between BRDF and vegetation structure," *Int. J. Remote Sens.*, vol. 23, pp. 2767–2796, 2002.

[8] M. J. Chopping, A. Rango, K. M. Havstad, F. R. Schiebe, J. C. Ritchie, T. J. Schmugge, A. N. French, L. Su, L. McKee, and R. Davis, "Canopy attributes of desert grasslands and transition communities derived from multi-angular airborne imagery," *Remote Sens. Environ.*, vol. 85, pp. 339–354, 2003.

[9] J.-L. Widlowski, B. Pinty, N. Gobron, M. M. Verstraete, D. J. Diner, and A. B. Davis, "Canopy structure parameters derived from multi-angular remote sensing data for terrestrial carbon studies," *Clim. Change*, vol. 67, pp. 403–415, 2004.

[10] R. M. Welch and B. A. Wielicki, "Stratocumulus cloud field reflected fluxes: The effect of cloud shape," *J. Atmos. Sci.*, vol. 41, pp. 3085–3103, 1984.

[11] R. Cahalan, W. Ridgeway, and W. J. Wiscombe, "Independent pixel and Monte Carlo estimates of stratocumulus albedo," *J. Atmos. Sci.*, vol. 51, pp. 3776–3790, 1994.

[12] A. Marshak, A. Davis, W. Wiscombe, and G. Titov, "The verisimilitude of the independent pixel approximation used in cloud remote sensing," *Remote Sens. Environ.*, vol. 52, pp. 71–78, 1995.

[13] N. G. Loeb, T. Várnai, and R. Davies, "Effect of cloud inhomogeneities on the solar zenith angle dependence of nadir reflectance," *J. Geophys. Res.*, vol. 102, pp. 9387–9395, 1997.

[14] P. Zuidema and F. K. Evans, "On the validity of the independent pixel approximation for boundary layer clouds observed during ASTEX," *J. Geophys. Res.*, vol. 103, pp. 6059–6074, 1998.

[15] B. Pinty, N. Gobron, J.-L. Widlowski, T. Lavergne, and M. M. Verstraete, "Synergy between 1-D and 3-D radiation transfer models to retrieve vegetation canopy properties from remote sensing data," *J. Geophys. Res.*, vol. 109, 2004.

[16] Y. Govaerts and M. M. Verstraete, "Raytran: A Monte Carlo ray-tracing model to compute light scattering in three-dimensional heterogeneous media," *IEEE Trans. Geosci. Remote Sens.*, vol. 36, no. 2, pp. 493–505, Mar. 1998.

[17] R. L. Thompson and N. S. Goel, "Two models for rapidly calculating bidirectional reflectance: Photon spread (PS) model and statistical photon spread (SPS) model," *Remote Sens. Rev.*, vol. 16, pp. 157–207, 1998.

[18] J.-L. Widlowski, T. Lavergne, B. Pinty, M. M. Verstraete, and N. Gobron, *Rayspread: A Virtual Laboratory for Rapid BRF Simulations Over 3-D Plant Canopies*, ser. Lectures Notes in Computational Science and Engineering. Berlin, Germany: Springer-Verlag, 2005.

[19] J.-L. Widlowski, B. Pinty, N. Gobron, and M. M. Verstraete, "Allometric relationships of selected European tree species," EC Joint Res. Centre, Ispra, Italy, Tech. Rep. EUR 20855 EN, 2003.

[20] N. Gobron, B. Pinty, M. M. Verstraete, and Y. Govaerts, "A semi-discrete model for the scattering of light by vegetation," *J. Geophys. Res.*, vol. 102, pp. 9431–9446, 1997.
[21] B. Hapke, "Bidirectional reflectance spectroscopy. I. Theory," *J. Geophys. Res.*, vol. 86, pp. 3039–3054, 1981.
[22] S. A. W. Gerstl, "Angular reflectance signature of the canopy hotspot in the optical regime," in *4th Int. Coll. Spectral Signatures of Objects in Remote Sensing*, Aussois, France, 1988, ESA Rep. SP-287, pp. 129–129.
[23] M. M. Verstraete, B. Pinty, and R. E. Dickinson, "A physical model of the bidirectional reflectance of vegetation canopies. 1. Theory," *J. Geophys. Res.*, vol. 95, pp. 11 765–11 775, 1990.
[24] R. Meerkoetter, "Reflection functions for inhomogeneous land surfaces," *Appl. Opt.*, vol. 29, pp. 4192–4198, 1989.
[25] W. Qin and Y. Xiang, "On the hotspot effect of leaf canopies: Modeling study and influence of leaf shape," *Remote Sens. Environ.*, vol. 50, pp. 95–106, 1994.
[26] N. S. Goel, W. Qin, and B. Wang, "On the estimation of leaf size and crown geometry for tree canopies from hotspot observations," *J. Geophys. Res.*, vol. 102, pp. 29 543–29 554, 1997.
[27] B. Pinty, J.-L. Widlowski, N. Gobron, and M. M. Verstraete, "Uniqueness of multi-angular information—Part 1: A surface heterogeneity indicator from MISR," *IEEE Trans. Geosci. Remote Sens.*, vol. 40, no. 7, pp. 1560–1573, Jul. 2002.
[28] H. Rahman, M. M. Verstraete, and B. Pinty, "Coupled surface-atmosphere reflectance (CSAR) model. 1. Model description and inversion on synthetic data," *J. Geophys. Res.*, vol. 98, pp. 20 779–20 789, 1993.
[29] N. Gobron and D. Lajas, "A new inversion scheme for the RPV model," *Can. J. Remote Sens.*, vol. 28, pp. 156–167, 2002.
[30] N. Gobron, B. Pinty, and M. M. Verstraete, "Theoretical limits to the estimation of the leaf area index on the basis of visible and near-infrared remote sensing data," *IEEE Trans. Geosci. Remote Sens.*, vol. 35, no. 6, pp. 1438–1445, Nov. 1997.
[31] J. Ross, *The Radiation Regime and Architecture of Plant Stands*. Boston, MA: Dr. W. Junk, 1981.
[32] N. Widen, "Assessing the accuracy of land surface characteristics estimated from multi-angular remotely sensed data," *Int. J. Remote Sens.*, vol. 25, pp. 1105–1117, 2004.
[33] R. Cahalan, W. Ridgeway, W. J. Wiscombe, and T. Bell, "The albedo of fractal stratocumulus clouds," *J. Atmos. Sci.*, vol. 51, pp. 2434–2455, 1994.
[34] A. Marshak, A. Davis, R. F. Cahalan, and W. Wiscombe, "Nonlocal independent pixel approximation: Direct and inverse problems," *IEEE Trans. Geosci. Remote Sens.*, vol. 36, no. 1, pp. 192–205, Jan. 1998.
[35] B. Cairns, A. Lacis, and B. Carlson, "Absorption within inhomogeneous clouds and its parameterization in general circulation models," *J. Atmos. Sci.*, vol. 57, pp. 700–714, 2000.
[36] G. W. Petty, "Area-average solar radiative transfer in three-dimensional inhomogeneous clouds: The independently scattering cloudlet model," *J. Atmos. Sci.*, vol. 59, pp. 2910–2929, 2002.
[37] M. M. Verstraete and B. Pinty, "Radiation transfer in SVAT models," in *Land-Surface Parameterization/Soil Vegetation-Atmosphere Transfer Schemes Workshop*, H. Dolman and R. E. Dickinson, Eds., 1997, IGPO Publication Series 31: GEWEX Tech. Rep., pp. 31–39.
[38] B. Pinty, T. Lavergne, R. E. Dickinson, J.-L. Widlowski, N. Gobron, and M. M. Verstraete, "Simplifying the interaction of land surfaces with radiation for relating remote sensing products to climate models," J. Geophys. Res., 2005, submitted for publication.

Jean-Luc Widlowski received the B.Sc. degree in geophysics and planetary physics from the University of Newcastle upon Tyne, U.K., the M.Sc. degree in remote sensing and image processing technology from the University of Edinburgh, Edinburgh, U.K., and the Ph.D. degree from the University of Fribourg, Fribourg, Switzerland, in 1993, 1995, and 2002, respectively.

He is currently with the Institute for Environment and Sustainability, Ispra, Italy, coordinating the RAdiative transfer Model Intercomparison (RAMI) activity (http://rami-benchmark.jrc.it/), and developing advanced methods for the extraction of quantitative information on terrestrial surface heterogeneity at the subpixel scale.

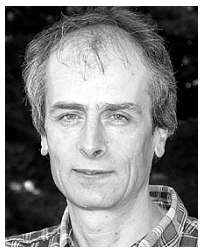

Bernard Pinty received the Maitrise de Chimie and DEA degrees, the thèse de troisieme cycle en physique de l'atmosphère, and the thèse d'Etat, in 1977, 1980, and 1988, all from the Université Blaise Pascal, Clermont-Ferrand, France.

He has visited the National Center for Atmospheric Research, Boulder, CO (1988–1989), served as Deputy Director of the Laboratoire d'Etudes et de Recherches en Teledetection Spatiale, Toulouse, France (1990–1992), and was appointed Full Professor of physics at the Universite Blaise Pascal in 1993. He is currently with the Institute for Environment and Sustainability, Ispra, Italy. He is a member of the MERIS Scientific Advisory Group of the European Space Agency and a member of the MISR Science Team of NASA/JPL. His main interests currently include research on the theory of radiation transfer over land surfaces, and, more generally, the development of tools to quantitatively interpret satellite remote sensing data in the solar spectral domain.

Dr. Pinty received the Zel'dovich medal from COSPAR in 1990.

Thomas Lavergne received the diplome d'ingenieur en mathématiques et méthodes numériques from the Institut des Sciences Appliquées, Toulouse, France, in 2003.

He worked during short collaboration periods at Onera, Toulouse, France, EUMETSAT, Darmstadt, Germany, and IFREMER, Brest, France, on the modeling of radiation transfer and on the validation of remote sensing data. He is currently with the Institute for Environment and Sustainability, Ispra, Italy, implementing advanced 3-D radiative transfer modeling and inversion schemes to retrieve vegetation canopy properties from optical remote sensing data.

Michel Max Verstraete (M'95–SM'03) received the License en Physique from the Université Catholique de Louvain, Louvain-la-Neuve, Belgium, the License Spéciale en Géophysique from the Université Libre de Bruxelles, Brussels, Belgium, and the M.Sc. degree in meteorology and D.Sc. degree in atmospheric sciences from the Massachusetts Institute of Technology, Cambridge, in 1974, 1976, 1978, and 1985, respectively.

He was with the World Meteorological Organization, Geneva, Switzerland and Nairobi, Kenya (1979–1981); at the National Center for Atmospheric Research, Boulder, CO (1982–1989); taught at the University of Michigan, Ann Arbor (1989–1990); and is currently employed at the Institute for Environment and Sustainability of the EC Joint Research Centre, Ispra, Italy. He is a member of various scientific advisory committees (e.g., MERIS) of the European Space Agency and Coinvestigator on the MISR Science Team of NASA/JPL. His initial work on topics such as the modeling of atmosphere–biosphere interactions and desertification led him to his current interest in the quantitative exploitation of satellite remote sensing data for the characterization of terrestrial surface properties.

Nadine Gobron (M'01) received the Maitrise de Physique degree, the DEA degree in sciences de la terre et de l'atmosphere, and the doctorat d'université en physique de l'atmosphere in 1993, 1994, and 1997, respectively.

She joined the DG Joint Research Centre, Ispra, Italy, in 2000. She is currently a Physicist from the Université Blaise Pascal, Clermont-Ferrand (France). She is now working as a Research Scientist to exploit remote sensing data to characterize the state and evolution of terrestrial environments. She is currently acting as Vice-Chair of commission A3 Land Processes and Morphology of the Committee on Space Research (COSPAR).